LAWRENCE
LIVERMORE
NATIONAL
LABORATORY

LLNL-JRNL-665251

Instability Growth Seeded by Oxygen in CH Shells on the National Ignition Facility

S. W. Haan

December 10, 2014

Physics of Plasmas

Disclaimer

Instability Growth Seeded by Oxygen in CH Shells on the National Ignition Facility

S. W. Haan,[1] H. Huang,[2] M. A. Johnson,[1] M. Stadermann,[1] S. Baxamusa,[1] S. Bhandarkar,[1] D. S. Clark,[1] V. Smalyuk,[1] H.F. Robey[1]

[1]Lawrence Livermore National Laboratory, P.O. Box 808, Livermore, California 94550, USA

[2]General Atomics, P.O. Box 85608, San Diego, California 92186, USA

Manuscript date Nov. 21, 2014

This work performed under the auspices of the U.S. Department of Energy by Lawrence Livermore National Laboratory under Contract DE-AC52-07NA27344.

ABSTRACT

Fusion targets imploded on the National Ignition Facility are subject to hydrodynamic instabilities. These have generally been assumed to be seeded primarily by surface roughness, as existing work had suggested that internal inhomogeneity was small enough not to contribute significantly. New simulations presented here examine this in more detail, and consider modulations in internal oxygen content in CH plastic ablators. The oxygen is configured in a way motivated by measurement of oxygen in the shells. We find that plausible oxygen nonuniformity, motivated by target characterization experiments, seeds instability growth that is 3-5x bigger than from a surface ripple or a density nonuniformity with the same initial column density modulation. Pertinent existing capsule characterization is discussed, which suggests the presence of internal modulations that could be oxygen at levels large enough to be the dominant seed for hydrodynamic instability growth. Oxygen-seeded growth is smaller for implosions driven by high-foot pulse shapes, consistent with the performance improvement seen with these pulse shapes. Growth is somewhat smaller for planned future pulse shapes that were optimized to minimize growth of surface ripples. A possible modified specification for oxygen modulations is discussed, which is about 1/5 of the current requirement.

I. INTRODUCTION

Implosions of fusion capsules at the National Ignition Facility[1] are susceptible to hydrodynamic instabilities seeded by any initial asphericities in the capsule. Prior work has concentrated on surface roughness as the seed for these instabilities, although it has been known that bulk irregularities in density or composition can also seed instability growth.[2] Target characterization and simulations of density modulations were taken to imply that bulk inhomogeneities were small enough that the growth was dominated by surface roughness. This report describes new simulations, which find that growth seeded by nonuniformity in oxygen content is larger than had been previously assumed. Existing characterization work is described, which allows the existence of problematic levels of oygen nonuniformity.

Some of the existing characterization suggests a level of nonuniformity that could result in perturbations several-times larger than the expected growth from surface roughness. Existing characterization does not directly indicate whether or not the observed nonuniformity is due to oxygen, so we cannot say at this time that the effect presented here has been proven to be important to NIF implosions. The point at this time is that dangerous levels of oxygen modulation are consistent with all existing information, both from target characterization and NIF implosion performance; they were not adequately specified, so the requisite characterization work has not yet been done. Hence, they are an important hypothesis to be pursued with both better characterization, and experiments on Omega and/or NIF.

The targets being discussed here have the geometry shown in Fig. 1. The targets are indirectly driven: the Au cylinder is heated by laser beams coming through entrance holes at the ends of the cylinder, and fills with nearly-Planckian x-rays coming to a peak radiation temperature of about 300eV. The detailed temporal history depends on the laser pulse; the histories discussed herein are shown in Fig. 2. The fusion fuel in the center is enclosed in a shell called the ablator, which is made of a CH plastic called Glow Discharge Polymer (GDP). Deposition of the nearly-Planckian x-rays in the GDP ablator drives the implosion of the DT fuel along with some remaining GDP. The implosion is hydrodynamically unstable and considerable work has gone into quantifying the growth of these instabilities. Most of the work specifying the seeds for the hydrodynamic instabilities[2] has assumed that the growing perturbations are initially seeded by ripples on the material interfaces in the capsule, as is typically the case for Rayleigh-Taylor and Richtmyer-Meshkov interface instabilities. However, these instabilities can also be seeded with modulations in density or composition; the perturbations then grow on the unstable interfaces (primarily the ablation front) and eventually have all of the same characteristics as perturbations seeded on the interfaces. The possibility of these seeds has been considered previously—for example, ref. 2 mentions them briefly as they are constrained by the Precision Radiography[3] (PR) characterization measurement discussed further below. There have been requirements in place for both density modulations and oxygen modulations. However, the point of this work is that those requirements, and the associated target characterization procedures, were not adequate to ensure that the modulations did not affect the implosion significantly.

The capsules are required to be very smooth. The smoothness is characterized with Atomic Force Microscopy,[4] and an optical interferometric instrument called Phase Shifting Diffractive Interferometry (PSDI).[5] The surface often has numerous dome-shaped protrusions typically 100's of nm high and 20-30 μm wide. Other than the larger domes, the smoothness is generally characterized with a power spectrum in Fourier modes, where mode 1 corresponds to a wavelength equal to one full circumference of the shell. Specific requirements will be discussed below, in the context of what oxygen modulations have equivalent impact.

Implosions of fusion ignition targets in the National Ignition Campaign often performed as if the shells experienced late-time hydrodynamic perturbation amplitudes that were several-times larger than expected from the growth of surface

roughness perturbations.[5,6] This was characteristic of both cryogenic layered implosions[5] and gas-filled single shell implosions.[7,8] Mix of ablator material into the hot-spot was also sometimes greater than expected for the NIC low-foot implosions,[9] which again suggests the pattern of larger-than-expected hydrodynamic perturbations. Targets driven with a high-foot pulse shape, which has less instability growth,[10] performed considerably closer to expectations from simulations.[11,12] Since the high-foot implosions are less unstable hydrodynamically, their better performance is often taken to confirm a pattern that the implosions generally are somewhat more susceptible than expected to hydrodynamic perturbations. On the other hand, direct measurements of the instability growth have been quite close to what was expected from simulations.[13,14,15] The modulations in these direct measurements are large, to allow measurement of their growth: they are large-amplitude grooves, uniform in one direction so that the data can be averaged along the groove and reduce experimental noise. Because of the large initial amplitudes, the intentionally-seeded perturbations dominate what grows from residual 3D features. Thus these experiments would be blind to oxygen-seeded growth even if it is larger than the growth from nominally smooth surfaces. Remarkably, shortly after the oxygen-seeded work described here was developed, direct measurements of 3D perturbation growth from nominally smooth capsules indicated larger amplitudes than would result from surface roughness alone, with growing perturbations that do not correlate with initial surface roughness features.[16,17] Some of the observed perturbations are remarkably structured, which suggests that they are produced by a non-random process during fabrication. Overall, then, the pattern is that the growth of large-amplitude imposed surface perturbations is confirmed to be close to simulations, but when the surface perturbations are small enough to be comparable to the ignition target smoothness requirements, then the final amplitudes are larger than expected from the known target features. This suggests an additional seed to hydrodynamic instabilities. This paper describes the impact of irregularity in the oxygen in the ablator, as such a seed. (We also discuss density modulations, which we will show to be less important.) We find that very plausible oxygen modulations, which are consistent with target characterization measurements by the target fabrication team as discussed below, can cause perturbation growth that is several-times larger than the nominally smooth surface features.

To quote ref. 18: "It is well known that GDP contains free radicals as a result of the deposition process.[19] These free radicals provide bonding sites for oxygen.[20,21]" The density of free radicals, and subsequently oxygen, is known to depend on exposure of the GDP to x-rays.[18] Ultraviolet irradiation, which is commonly used for curing epoxy during target fabrication, almost certainly also causes free radicals and subsequent oxygen pickup. The amount of bulk oxygen is known to depend on the history of the capsule and the diffusivity of water molecules in the GDP.[22] The hypothesis presented here is that the known oxygen content has modulations transverse to the capsule radius that are small enough to have almost escaped measurement, but large enough to be important to capsule performance. The hypothesized modulations in oxygen content are very small (about 0.01 at%, out of the 2-5 at% that is known to be present near the outer surface). GDP is known

to be slightly porous, and to have qualities sensitive to handling and processing,[23] and to vary in density from shell to shell. Shells have surface irregularities and roughness that are comparable to the isocontours of the oxygen levels hypothesized here. It has been noted that the GDP has structural irregularity under the surface domes,[24] which could provide sites for more (or less) oxygen bonding. It does not seem at all implausible that small modulations in composition are present in a polymeric structured material such as GDP, with known affinity for oxygen. It is unfortunate that the importance of this was not recognized years ago, so that an appropriate requirement would have driven the necessary characterization work. In the following we will occasionally contrast our original thinking on these topics with the current work.

In the following, we describe the best estimates that are available from target characterization of the oxygen content and profile, and use these measurements to assemble a nominal model for the oxygen contamination as a function of position in the ablator. Simulations with the code Laxnex[25] were done of this model, and for variants on it. These simulations indicate that growth from modulations in oxygen concentration are larger than had been expected, and are likely to be a significant seed for instability growth. The current best estimate of the size of the resulting perturbations is that they are likely to be somewhat larger than the familiar perturbations seeded from surface ripples (effectively, equivalent to a factor of about 2-3 multiplier on the surface roughness). Detailed measurements of the oxygen contamination are clearly important, and it is hoped that some months from now a fully-justified description will be available to put into more detailed simulations. The results presented here are intended to provide a context for future oxygen-contamination measurements, as regards what features of the contamination are most important to quantify.

Simulations described below also indicate that high-foot implosions[10,11,12] have less growth than low-foot implosions when seeded with oxygen modulations, just as they are known to have less growth when seeded with surface ripples, both in simulations[10] and experiments.[14] The better performance of the high-foot implosions is then consistent with the hypothesis that the oxygen modulations are a major source of perturbation growth for the implosions. A third class of NIF implosions is being developed with high-picket pulses (sometimes called “adiabat-shaping”) which were designed so that they have less growth as seeded by the usual outer surface roughness.[26, 27, 28] As described below, these are somewhat less sensitive to the oxygen modulations than the NIC low-foot pulses, although not necessarily so much so as the high-foot.

II. CHARACTERIZATION OF OXYGEN PROFILES IN GDP SHELLS

The shells under discussion are made by coating CH in a GDP process on a mandrel made of another plastic PAMS.[29] The mandrel is then removed by thermal permeation at ~300°C for about one day. The GDP material is polymeric C and H at a C:H ratio of about 43:57. The shells are sometimes polished, in aqueous bath, or can be used unpolished if they are smooth enough. Insofar as it is possible without extraordinary measures, they have been protected from oxygen exposure during

storage and transport. Some exposure occurs for example during characterization and polishing, and assembly into the hohlraum. From modeling that successfully describes the oxygen features described below, it is indicated that the oxygen residing in the shell enters as water, while dry molecular O_2 diffuses more freely through the shell but does bind into place.[22] The amount of oxygen in the shells is weakly dependent on exposure history.

Three measurements have been done in target characterization that inform our description of oxygen in the GDP:

1. Radial profile via contact radiography.

The radial dependence of oxygen in the GDP has been measured by projection x-ray imaging, described in Ref. 22. There are three features of the radial oxygen profile: (i) Deep in the shell, the oxygen is approximately uniform at a level that varies from shell to shell, and is around 0.3 to 0.8 at%. (ii) There are brief excursions, at particular radii, by an additional ~0.5 at%, a few microns thick, that occur when the coating process is interrupted for some reason and the capsule is exposed to air when the layer has not yet reached full thickness. (iii) At the outer surface, the oxygen ramps up to a higher level of 2-5 at%, over a scale length of 20-30μm. It is a reasonable fit to approximate the outer ramp with an exponential, and a typical profile that will be used here for the oxygen atomic percent is

$$O_{at\%} = 0.5 + 3e^{-d/30\mu m} \qquad (1)$$

Here d is the distance from the outer surface of the ablator. It is likely that the inner surface has a similar ramp, but as we will describe below this does not seed significant growth and is ignored here. The actual scale length varies around 20-40μm, and the outermost maximum level varies around 2-5 at%. The maximum level is related to the storage history of the shell. It is worth noting that the oxygen profiles for different measurements on a particular shell as shown in ref. 22 typically vary from curve to curve by 0.2 to 0.5 at%, which could be pure statistical noise or could represent actual variations from place to place around the shell. The variations are somewhat coherent from trace to trace, that is, a trace that is higher at one radius tend to be higher at other radii, but only weakly so. The authors note that the variability increases with oxygen fraction and can be represented as (in units of at%) 0.17+0.13 x O_at%. This is represented as noise; for our purposes, it can be taken as a bound on lateral variations, and perhaps a rough estimate if the lateral variations are large enough to appear in this diagnostic. The stated conclusion of these measurements as regards lateral variations is that the GDP is "uniform within the accuracy of the measurement."

This radial profile has been known for some time, and its implications for 1D shock timing were explored in simulations--for example, in ref. 30, it was noted that a 2at% oxygen profile such as eq. (1) would delay the first shock by about 50ps, or the equivalent of a 1.5 micron thickness difference if the shock velocity is 30 μm/ns. Thus a 0.02at% modulation would be roughly equivalent to 15nm, about a factor of 5 smaller than is seen in the simulations presented below. This additional factor results from the RM growth seeded by the oxygen modulation.

The radial profile only slightly affects the seeding of instability growth by modulations in the oxygen level. This sensitivity is discussed below when we discuss the growth simulations. We emphasize that the effect of the oxygen is *not* to change the instability growth—the usual parameters such as density profiles and ablation velocities, which affect the growth, are not significantly changed by the oxygen profiles under discussion here. The phenomenon being discussed here is simply the growth of perturbations seeded by modulations in oxygen content, not any significant effect of oxygen on the growth.

2. Internal structure via PSDI.

In order to measure lateral inhomogeneity, interferometric measurements were done in 2010 by one of the authors (M.A. Johnson). An instrument that is regularly used for surface characterization, Phase-Shifting Diffraction Interferometer (PSDI),[31] was configured to measure the shift in phase of optical 532nm light when the light is transmitted through the spherical shell. Typically PSDI uses light reflected from the capsule surface, using the phase shift of the reflected light to measure surface features. In transmission mode, PSDI can measure the integral of the refractive index, on passage along a ray through both sides of the shell. Lateral resolution is about 5 microns, although in this transmission mode on the shells used in the experiment, the noise dominates the signal for wavelengths smaller than about 25 microns. The measurement is sensitive to optical depth variations that are equivalent to about 1nm of surface ripple. The measurements are images of patches of the shell, about 400 μm in diameter. The phase shift of transmitted light is determined by both surface features and any internal modulations in refractive index. It can be reported as "equivalent surface roughness" by calculating the surface roughness that would cause the observed phase shift. The refractive index surplus, n-1, is estimated to proportional to density, and the measurement can be interpreted as "net column density." We are most interested in possible oxygen contributions, which can be connected to this data via two facts: (i) it has been determined by separate measurements that oxygen increases the density of GDP according to

$$\rho = \rho_0 + 0.029 * O_{at\%} \quad (g/cc); \tag{2}$$

and (ii) the increase in refractive index that results from addition of oxygen is estimated to be linear with mass density, with little significance difference in $n(\rho)$ between a density increase due to oxygen or due to some other change in structure. Finally, to estimate the contribution from internal structure as opposed to surface roughness, the surface was measured separately with conventional reflective PSDI.

Fig. 3 shows the power spectrum from these optical transmission measurements, reported as "equivalent surface roughness." There are three measurements (each a separate 400μm diameter "medallion") from three shells. Fig. 3 also shows, labeled "NIF surface spec," the power spectrum that would be expected for this measurment if the outer surface roughness of the shells that were used had been equal to the outer surface roughness specification. The measured modulations in optical depth are well below this surface roughness equivalent, and

at the time of these experiments this was taken to indicate that the GDP did not have unacceptable internal density modulations. (More detailed analysis of that question is the focus of the current work, as discussed below.) Fig. 3 also shows a gray band, for comparison to Fig. 4, which shows the measured actual outer surface roughness of these shells. (Fig. 4 does not include a noise curve, but it is known that the noise for conventional reflective PSDI is well below these measurements.) We see that the measured modulations in optical depth in Fig. 3 are somewhat above the modulations expected from surface roughness alone, indicating the presence of small modulations in bulk optical depth. (Or inner surface modulations, as discussed below.) This is most clearly true around modes 100-300; at modes above about 300 the transmission measurement is falling to its noise level and is unreliable, while below mode 100 the difference between optical depth and surface is questionable. The inner surface, for which we have no data and which we ignore in this discussion, also modulates the optical depth. Inner surfaces tend to be very smooth and neglecting the inner surface is defensible albeit not definitively justifiable. Thus, while this data does not provide a fully adequate measurement of the optical depth modulations, it does provide an indication that optical depth modulations are present, and a rough estimate of their possible magnitude. At mode 200, for example, the power spectrum of the optical depth modulations is about 1-5 $x10^{-2}$ nm^2 equivalent. At mode 60, it is smaller than 0.25 nm^2 equivalent, and may be about 0.1 nm^2.

Fig. 3 includes a solid curve, which is a test case we will follow in the rest of this article. This is surface-roughness-equivalent power spectrum

$$P_{test1D}(nm^2) = (10/mode)^{1.1}\, e^{-(\frac{mode}{1000})^2}\,. \qquad (3)$$

(Note that there is an implicity normalization to the data in this expression, which happens to be $1nm^2$.) It would be premature to call this a "measured" level of internal modulations, and it is certainly a conjecture to associate this with oxygen modulations. At this time this is just a benchmark. The magnitude and slope are suggested by the Johnson optical depth data; the exponential falloff at large mode is for convenience in calculating transforms, and has no effect on the analysis below. Note that this power spectrum is considerably below what we had envisioned as the requirement at the time that Johnson did this work, which would be perhaps ½ the black "NIF surface spec" curve in Fig. 3.

Although we have not included a figure of the real-space experimental images that correspond to these power spectra, we note that the real-space data does not show any noteworthy features or structure. Artificial data that is reconstructed from a plausible power spectrum such as eq. (3), assuming random phases for all modes, has peak-to-valley and other statistical features very similar to the actual real-space data. Thus, there is no indication that the optical-depth modulations in these shells had particular structure in the transverse direction, beyond what one would model with a randomly-phased reconstruction from the power spectrum.

In Sec. IV below we will construct a model for oxygen in the GDP that is consistent with these data, after discussing the other measurement that constrains our modeling.

3. Internal structure via Precision Radiography

The homogeneity of GDP has also been measured via transmission of 6-10 keV x-rays, in a system known as Precision Radiography (PR).[3,18] This system provides measurements accurate to 1:10^4 of the optical depth to the x-rays, upon transmission through both sides of the capsule. The x-ray energy used varies with application; recent work has used a broad-band 6-10 keV source. Measurements to date on GDP have returned results consistent with the surface roughness requirements, which is around the noise limit for the measurement. PR has limited spatial resolution, and is limited to modes below about 50. To date, then, PR has not constrained the oxygen content more tightly than the PSDI measurement. Oxygen has about 2.8x more opacity to the x-rays than the GDP bulk, per unit density. This suggests that measurement on very smooth shells, such as those shown in Figs. 3 and 4, might return an indication of internal modulations, if this can be measured beyond the noise limitations. This also suggests that PR could return useful data on the oxygen modulations, since this sensitivity factor is very similar to the relative amplification by the growth factors presented below.

To date we do not have sufficiently systematic PR data to present here. It is known that PR disrupts the GDP, so it is a destructive measurement and is typically not done on GDP shells. Also, the X-ray absorption is very sensitive to the Si or Ge dopant, and to the roughness of the interfaces between the different levels of dopant. This internal interface roughness appears to dominate the modulations seen in existing data.

Ref. 18 describes how PR can be used intentionally to introduce oxygen-modulations into the GDP. When part of a GDP shell is exposed to the PR x-rays, and then the shell is subsequently recharacterized, it is found the exposed material has higher optical density. In Ref. 18 this is inferred to be because the x-rays create free radicals, to which oxygen then binds. In the experiment described in Ref. 18 this reduced the x-ray transmission by about 0.4%, corresponding to 0.18 at% oxygen if it is radially uniform in the shell. According to the simulations presented below, this would seed the same instability growth as a micron-scale surface step, which would be very easy to see in a Rayleigh-Taylor experiment. Similar effects almost certainly occur from exposure to ultraviolet radiation, which commonly occurs during target assembly because the targets are assembled with UV-cure epoxy.

III. SIMULATIONS OF GROWTH SEEDED BY OXYGEN MODULATIONS

We have used the radiation-hydrodynamics code Lasnex[25] to simulate instability growth seeded with oxygen modulations, simply by having the oxygen present as a minor ingredient in the GDP and varying it spatially. As soon as the contaminated material experiences radiation or hydrodynamics, velocity and spatial modulations begin to grow. For the work presented here, the simulations were typically done with one half of a single transverse wave of a Legendre-polynomial single mode perturbation. This makes it straightforward to ensure linear dynamics,

and overall quality control on the evolution and dynamics. For these linear perturbations, the late-time evolution is the same regardless of how the perturbation was seeded—the rad-hydro evolves towards a radial eigenfunction of growth, and then the growth is the same regardless of seed. The amplitude with which the perturbation finally grows is the key parameter.

In most of the simulations described here, the density is modulated in correspondence with the oxygen, following eq. (2) above. (Simulations were also done in which the density alone is modulated, and others in which the concentration alone is modulated, described below.) Modulating them together allows a calibration against surface ripple simulations, by matching column density. In the low mode limit where the differential velocity simply results from the modulation in the mass in *f=ma*, matching the column density matches the impact of the perturbation.

The simulations are run with standard scaling of the opacities (using mixed opacities from the OPAL code[32]) and equation of state (using Thomas-Fermi scaling[33,34] for the small deviations from the tabulated pure-GDP EOS[35]). In the part of the problem where the oxygen varies, each transverse zone thus has a slightly different opacity and EOS. In the baseline model, eq. (2) is also used to modulate the density along with the oxygen content. These simulations can then be normalized to surface ripple simulations with the same column density modulation. Simulations were generally run Lagrangian so that the oxygen-modulated material is simply tracked. The simulations described here were capsule only, driven with a frequency-dependent radiation source. Most of the simulations described below used a source (curve (i) in Fig. 2) where the shocks were tuned to replicate the best-tuned NIC shot N120329. The final rise of the source was increased to achieve ignition-like velocities without increasing the adiabat. The various other drives in Fig. 2 are discussed below.

We simulated various radial dependences for the oxygen modulation.

One radial dependence for the oxygen modulation in the simulation is suggested by the radial profile eq. (2). The modulation is placed on the oxygen penetrating near the outer surface:

$$O_{at\%} = 0.5 + 3e^{-\frac{d}{30}}\{1 + \varepsilon P_l(cos\theta)\}. \qquad (4)$$

The perturbation that grows is proportional to ε provided ε is small enough that the ultimate perturbation is linear by the usual standards. Fig. 5 shows the growth factor vs. mode number for this oxygen seed, along with a few variants. The quantity plotted is the growth factor in fractional column density, taking the modulation ρR(mod)/ ρR(avg) in ρR at peak velocity, divided by the initial relative ρR modulation. With this same normalization, Fig. 5 includes the growth of perturbations seeded by the usual surface ripples. (For the modes that grow significantly in this work, the final perturbation has the same radial dependence regardless of seed. Thus any of the definitions of growth factor can be scaled to oxygen seeds, in proportion to the curves in Fig. 5.) In order to separate how much of the oxygen-seeded growth is due to the density increase given by eq. (2), Fig. 5 shows simulations that were done with density modulations alone, with the same spatial dependence as eq. (4). Finally, the oxygen composition modulation can be

simulated, without the density modulation. This requires normalization: Fig. 5 shows oxygen-only content modulation that is the same as the full oxygen-and-density case, for which ρR can be matched to a surface ripple. Several things are evident from Fig. 5. The case with density modulations alone almost matches the surface-ripple case, as one might expect. The case with oxygen modulations alone seeds a somewhat larger perturbation; the growing perturbation first appears in the simulation as a velocity modulation, with faster ablation and higher velocity where there is less oxygen. The case with combined oxygen and density, which is our best approximation to the actual net perturbation from the oxygen, is nicely thought of as the sum of these two effects.

In addition to this baseline scenario, it is also useful to know where the oxygen matters. This can be done with simulations in which the oxygen modulation is in a radial step of length b: the oxygen is taken to be

$$O_{at\%} = [0.5 + 3e^{-\frac{d}{30}}]\{1 + \varepsilon P_l(cos\theta)\mathrm{H}(b/2 - |d - d_0|)\} \qquad (5)$$

where H is the Heaviside step function. This is unity when d is within $\pm$b/2 of d_0 and is zero elsewhere. The amplitude ε is chosen to produce a modulation large enough to dominate numerical noise, and seed and grow sensibly, but small enough to ensure linearity. Various lengths b were run; the perturbation that is seeded is proportional to the length of the step, provided the length is small compared to other relevant scale lengths. A 2 to 5μm step provides a length that is resolvable but small enough that the perturbation is proportional to the length. Since the growing perturbation and the initial ρR modulation are both proportional to b, the growth can be normalized to the initial ρR modulation. This allows direct comparison with surface ripples. Fig. 6 shows the growth of these perturbations, normalized to initial ρR, at various depths d_0. It is notable that perturbations a few microns below the surface seed growth slightly more than perturbations right at the surface. At its worst—embedded by a few microns—the growth seeded by the thin layer is slightly larger than the $e^{-d/30}$ ramp, at equivalent ρR.

If the perturbed layer is deep in the shell, there is much less growth, and the processes that dominate the dynamics become different. The two curves in Fig. 6 actually cross—oxygen seeded perturbations grow *less* than equivalent density modulations, when the perturbed layer is close to the inner surface of the GDP. Detailed consideration of these deep layers is beyond the scope of this paper. Since the resulting perturbations are small, it is unlikely that they are important.

One might have expected that the oxygen would matter more when deeply buried, because it would directly feed into Rayleigh-Taylor growth. We find instead that there is more leverage connected with coupling to the Richtmyer-Meshkov phase. The modulations start the growth of a ρR modulation, which then grows to be a seed for the RT growth. The density modulations alone show this effect, with modulations just inside the shell being slightly worse than surface ripples. The velocity modulation launched by the opacity difference from oxygen adds coherently to the growth from the density modulation, making the combination considerably larger than had been expected prior to this work. For deeply

embedded perturbations, these two effects do not interact with the same dangerous coherence.

It is likely that oxygen modulations with arbitrary radial dependence can be calculated by integrating the product of the modulation profile times this curve, suitably normalized. This appears to be approximately consistent the $e^{-d/30}$ ramp, and is generally consistent with the trends in the simulations, although we have not attempted a detailed prescription along these lines. It is not obvious whether the accumulation of the perturbation during and following shock transit should be exactly linear in this sense, and we have not attempted the simulations needed to test this notion.

Another question is whether the various seeds have similar sensitivity to mode number. For the cases where the perturbation is seeded near the outside of the shell, such as shown in Fig. 5, the growth factor curves are very similar—peaking at mode 60 and falling off above mode 100. The more deeply seeded perturbations in Fig. 6 have a different shape, since the growth mechanism is less coupled to the ablation-front RM and RT growth. Since they grow much less, this is probably not an important effect.

Finally, we considered how the growth depends on the level of uniform background oxygen, for possible variations around eq. (1). The simulated growth, for given initial at% modulation, is a weakly decreasing function of the background oxygen level. If the exponential ramp in eq. (1) is eliminated, so that the background oxygen is flat at 0.5 at%, then the growth of a mode 60 modulation (which still has $e^{-d/30}$ radial dependence) is 8% larger; at the other extreme, if the 2 at% maximum radial level is increased to 5 at%, then the growth is 25% smaller. For example, a surface-level oxygen ripple 5 ± 0.1 at% will grow to the same peak-velocity perturbation as an initial oxygen ripple 2 ± 0.075 at%. One might have expected that the seeding would be proportional to the background level, which would have been a trend in the same direction but much steeper.

In summary, then, the simulations indicate that the growth can be as large as 4-5 times what is seeded by surface ripples of equivalent initial column density, depending on the radial structure of the oxygen modulation, with sensitivity to mode number that is similar to the familiar surface feature growth factor curves.

IV. AMPLITUDES RESULTING FROM A POSSIBLE OXYGEN CONFIGURATION

In this section we consider the net growth that would result, given the growth described in Sec. III, from the sorts of modulations suggested by target characterization as described in Sec. II.

As a representative structure, we consider the case where the radial dependence of the oxygen modulations is given by eq. (4) and the transverse modulations in integrated density have power spectrum given by eq. (3). The oxygen content is given by

$$O_{at\%} = 0.5 + 3e^{-\frac{d}{30}}\{1 + J_{test}(\theta, \phi)\} \qquad (6)$$

where $J_{test}(\theta, \phi)$ is a homogeneous isotropic randomly-phased function of lateral coordinates which is defined by the requirement that a lineout of column density has power spectrum eq. (3), with density following the oxygen modulation per eq. (2), and normalized to equivalent surface roughness. It is straightforward to construct realizations of this by adding randomly phased Fourier modes, for a small patch, or spherical harmonics for a larger segment of the sphere, with mode amplitudes adjusted so that a representative lineout has the specified power spectrum. The 2D power spectrum can also be calculated from the 1D-trace power spectrum by using the Pollaine-Hatchett transformation in ref. 36. The rms of a representative lineout can be uniquely determined by the power spectrum, while the rms of the full surface, and of other lineouts, fluctuate somewhat depending the realization. Note that the modulation is placed only on the outer exponential part, not on the deeper 0.5at% background.

It is interesting to note some features of this configuration. A transverse lineout of oxygen atomic % at the outer surface is shown in Fig. 7, over a 300μm length. The amount varies by about 0.02 at% around the average of 2 at%. Transverse lineouts deeper in the shell would be proportional to this curve, with the same shape but the magnitude and the modulations falling off together, exponentially into the shell. Radial lineouts at different transverse locations would be multiples of each other, with a constant multiplier varying by about 1% (i.e. 0.02 at% out of 2 at%). A 1 at% iso-oxygen contour has exactly the same shape as the surface profile plotted in Fig. 7, as shown with the right-hand scale in Fig. 7. The modulations in the iso-contour are about 100nm, only slightly larger than our specified surface roughness. It is likely that measuring such modulations in oxygen content will be very challenging.

This configuration grows to amplitudes somewhat larger than would be expected from surface roughness alone. The 2D power spectrum, obtained with the Pollaine-Hatchett transform,[36] is multiplied by the square of the growth factor curve in Fig. 5, and the result summed to get an rms. Table I presents the resulting rms, along with other cases of interest. This test-case oxygen-seeded growth is about 3x bigger than would result from the surface roughness of the shells in which these internal modulations were measured, and about 1.5x bigger than grows from the maximum allowed surface roughness.

For oxygen modulations somewhat smaller than being emphasized in this work—such as the draft requirement sketched below—the spatial variation of the iso-oxygen contours could be very similar in magnitude to the surface roughness. This raises a variety of subtle issues regarding how the surface roughness and the oxygen isocontours correspond in phase. Scenarios where the oxygen contours follow the surface roughness near the outer surface, but then smooth as one goes deeper in the shell, could serve as amplification factors on surface roughness. Working through such scenarios is beyond the scope of this work, which is centered on the hypothesis that current GDP capsules have oxygen somewhat larger and dominate the surface effects. It will be an important area of future work, as we strive to minimize the impact of the oxygen.

V. HIGH-FOOT AND HIGH-PICKET PULSE SHAPES

Experiments are being done with GDP on NIF with two other classes of pulse shapes, so called "high-foot"[11] and "high-picket."[26] With both of these new drives, experiments verify that there is less instability growth seeded by surface ripples.[14,27], as predicted by simulations.[15,10,26,28] For "high-foot" it is known that implosion experiments perform better than NIC "low-foot" pulses; experiments are in progress testing the performance of "high-picket" pulse shapes. The question arises, how these pulses change the sensitivity to the oxygen modulations considered here.

Frequency dependent sources for these cases, shown in Fig. 2, were used to simulate the growth in configurations that were otherwise identical. For "high-foot" we used a post-shot model for NIF shot N130927. For "high-picket" we used two sources: (i) a source as used in Ref. 26, based on a post-shot model for NIC low-foot shot N120329, but with increased picket per ref. 26; and (ii) a higher-velocity version with the same high-picket source for the first three shocks, but peak drive similar to the low-foot shot used for most of the work here. Fig. 2 shows the radiation history for the four sources used. (Although peak TR is lower for the two pulses (i) and (iv), the pulse is timed better with respect to the implosion, increasing the peak implosion velocity from 347 to 373 km/s. Implosion velocities and adiabats, as defined as in Ref. 2, are in Table 1 below.) Fig. 8 shows the growth for the three pulse shapes in consideration. Fig. 8a, for reference, shows simulations of conventional surface perturbations with the setup used here. The relative growth follows the trends expected from previous work. Fig. 8b shows the growth seeded by oxygen modulations using the profile in eq. (4) above. It is evident that the dramatic difference between low-foot and high-foot is the same for oxygen-seeded perturbations as it is for surface-ripple seeds. For the "high-picket" pulses it is a little more complicated; the original pulse from Clark shows only slightly more relative growth when seeded with oxygen modulations, but the more highly driven new pulse shows growth that is closer to the original low-foot pulse. As detailed in Ref. 26, the difference between the growth for implosions driven by these pulses is mostly in the phase of the Richtmyer-Meshkov growth, and the seeds for the RM phase are somewhat different when seeded by oxygen modulations rather than surface ripples. How these then couple to the acceleration phase depends on the 4th rise as well. The conclusion here is that "high-picket" pulses do have less growth when oxygen seeded than the NIC pulses, but the difference depends on details and it is not necessarily as big as the difference in growth seeded by a surface ripple.

VI. POSSIBLE REQUIREMENT ON OXYGEN MODULATIONS

It is useful to translate this work into requirements that target fabrication organizations can compare with characterization of the shells. One can envision two types of measurements that could be done: (i) integrated measurements of x-ray or optical transmission, such as discussed above; and (ii) actual measurements of local oxygen content. In the first category, we can see that existing measurement techniques are very close to being adequate, but the requirements that were in place were not tight enough. Tightening the existing requirements by a factor of about 5 in

power would ensure modulations with impact below that of surface roughness requirements, and allow good performance given the estimates presented here. Since Precision Radiography is dominated by the roughness of the internal dopant interfaces, and because it is destructive to the GDP, it is of limited value for shell characterization. It is more sensitive to oxygen than PSDI, and two of us (Huang and Johnson) have proposed a plan for using PR to calibrate the sensitivity of PSDI to oxygen modulations. Then PSDI could be used more extensively for characterization. The requirement would be that the integrated column density be ~1/25 of the "NIF spec" curve shown in Fig. 3. (A factor of 5 in amplitude being a factor of 25 in power.) This requirement could be loosened if we correspondingly reduced the allowed levels of surface roughness.

For explicit measurements of oxygen content and modulations, the requirement would be that the oxygen in the oxygen-rich layer, within 30 μm of the outer surface, have oxygen variations smaller than about half of those shown in Fig. 7—that is, smaller than about 0.005 at%. This could be translated into a power spectrum if data becomes available to evaluate quantitatively.

The level of modulation that matters depends on where it is radially, and on how far (in radius) the transverse modulations maintain phase. As a reference point point, we saw above that modulations of about 0.01 at% (Fig. 7), which persisted for 30μm near the outer surface caused perturbations about twice what we would want in a requirement (Table 1). Given the radial sensitivity shown in Fig. 6, we can estimate how large a modulation could be allowed as a function of where the modulation occurs in the shell, shown in Fig. 9.

Meeting these requirements would result in perturbations dominated (slightly) by surface roughness, as originally envisioned for NIF implosions. If the oxygen modulations remain perhaps a factor of two bigger than this, an improvement in final perturbations could be achieved by reducing surface roughness, trading off the two perturbation seeds. If the oxygen modulations are more than a factor of two bigger than this, the growth must be reduced by using pulse shapes that produce less growth.

For implosions with high-foot or "high-picket" pulse shapes, the requirements could be looser. Again, there is a tradeoff with surface roughness requirements, which could be similarly loosened. Details will depend on the final design, and on the levels of oxygen modulation that can be achieved.

V. SUMMARY

We have presented evidence from target characterization, and simulations, suggesting that modulations in oxygen content in GDP shells is an important seed for hydrodynamic instability growth. Estimated growth exceeds that seeded by surface roughness, by as much as a factor of several. Direct measurements of growing perturbations in recent NIF experiments also suggest the presence of a seed that dominates surface roughness, and which sometimes has structure suggestive of UV-induced oxygen modulations. Future experiments will need to have pulse shapes that reduce the sensitivity to these perturbations. Developing target characterization to measure the oxygen modulations will be very valuable.

TABLE 1. RMS perturbations resulting from the indicated scenarios, on the ablation front at peak velocity (μm). Peak velocity and adiabat for the four drives are included for reference.

	Low-foot drive	**High-foot drive**	**High-picket drive A**	**High-picket drive B**
Peak implosion velocity (μm/ns)	365	364	347	373
Adiabat	1.45	2.44	1.38	1.36
Seed:				
At-spec surface roughness alone	4.1	1.8	2.2	2.6
Measured surface roughness of shells characterized in Figs. 3 and 4	2.1	0.8	1.0	1.2
Oxygen modulations per eq. (6)	6.6	2.9	4.1	5.5

FIGURES see PPT file

REFERENCES

1. E. I. Moses, R. N. Boyd, B. A. Remington, C. J. Keane, and R. Al-Ayat, Phys. Plasmas **16**, 041006 (2009); G. H. Miller, E. I. Moses and C. R. Wuest, Opt. Eng. **443**, 2841 (2004).

2. S. W. Haan, J. D. Lindl, D. A. Callahan, D. S. Clark, J. D. Salmonson, B. A. Hammel, L. J. Atherton, R. C. Cook, M. J. Edwards, S. Glenzer, A. V. Hamza, S. P. Hatchett, M. C. Herrmann, D. E. Hinkel, D. D. Ho, H. Huang, O. S. Jones, J. Kline, G. Kyrala, O. L. Landen, B. J. MacGowan, M. M. Marinak, D. D. Meyerhofer, J. L. Milovich, K. A. Moreno, E. I. Moses, D. H. Munro, A. Nikroo, R. E. Olson, K. Peterson, S. M. Pollaine, J. E. Ralph, H. F. Robey, B. K. Spears, P. T. Springer, L. J. Suter, C. A. Thomas, R. P. Town, R. Vesey, S. V. Weber, H. L. Wilkens, and D. C. Wilson, Phys. Plasmas **18**, 051001 (2011).

3. S. A. Eddinger, R. B. Stephens, H. Huang,, T. J. Drake, A. Nikroo, G. Flint, and C. R. Bystedt, *Fusion Science and Technology **51**, 525 (2007).*

4. R. B. Stephens, D. Olson, H. Huang, and J. B. Gibson, *Fusion Science and Technology* **45**, 210 (2004).

5. R. C. Montesanti, M. A. Johnson, E. R. Mapoles, D. P. Atkinson, J. D. Hughes, and J. L. Reynolds, *Proc. American Society for Precision Engineering Annual Conf., Monterey, California*, October 15-20, 2006 (2006).

5. D. S. Clark, D. E. Hinkel, D. C. Eder, O. S. Jones, S. W. Haan, B. A. Hammel, M. M. Marinak, J. L. Milovich, H. F. Robey, L. J. Suter, and R. P. J. Town,
Phys. Plasmas **20**, 056318 (2013).

6. John Lindl, Otto Landen, John Edwards, Ed Moses and NIC Team, Phys. Plasmas **21**, 020501 (2014).

7. D. T. Casey, V. A. Smalyuk, R. E. Tipton, J. E. Pino, G. P. Grim, B. A. Remington, D. P. Rowley, S. V. Weber, M. Barrios, L. R. Benedetti, D. L. Bleuel, E. J. Bond, D. K. Bradley, J. A. Caggiano, D. A. Callahan, C. J. Cerjan, K. C. Chen, D. H. Edgell, M. J. Edwards, D. Fittinghoff, J. A. Frenje, M. Gatu-Johnson, V. Y. Glebov, S. Glenn, N. Guler, S. W. Haan, A. Hamza, R. Hatarik, H. W. Herrmann, D. Hoover, W. W. Hsing, N. Izumi, P. Kervin, S. Khan, J. D. Kilkenny, J. Kline, J. Knauer, G. Kyrala, O. L. Landen, T. Ma, A. G. MacPhee, J. M. McNaney, M. Mintz, A. Moore, A. Nikroo, A. Pak, T. Parham, R. Petrasso, H. G. Rinderknecht, D. B. Sayre, M. Schneider, W. Stoeffl, R. Tommasini, R. P. Town, K. Widmann, D. C. Wilson and C. B. Yeamans
Phys. Plasmas **21** , 092705 (2014).

8. S. V. Weber, D. T. Casey, D. C. Eder, J. D. Kilkenny, J. E. Pino, V. A. Smalyuk, G. P. Grim, B. A. Remington, D. P. Rowley, C. B. Yeamans, R. E. Tipton, M. Barrios, R. Benedetti, L. Berzak Hopkins, D. L. Bleuel, E. J. Bond, D. K. Bradley, J. A. Caggiano, D. A. Callahan, C. J. Cerjan, D. S. Clark, L. Divol, D. H. Edgell, M. J. Edwards, M. J. Eckart, D. Fittinghoff, J. A. Frenje, M. Gatu-Johnson, V. Y. Glebov, S. Glenn, N. Guler, S. W. Haan, A. Hamza, R. Hatarik, H. Herrmann, D. Hoover, W. W. Hsing, N. Izumi, O. S. Jones, M. Kervin, S. Khan, J. Kline, J. Knauer, A. Kritcher, G. Kyrala, O. L. Landen, S. Le Pape, T. Ma, A. J. Mackinnon, A. G. MacPhee, M. M. Marinak, J. M. Mcnaney, N. B. Meezan, F. E. Merrill, M. Mintz, A. Moore, D. H. Munro, A. Nikroo, A. Pak, T. Parham, R. Petrasso, H. G. Rinderknecht, D. B. Sayre, S. M. Sepke, B. K. Spears, W. Stoeffl, R. Tommasini, R. P. Town, P. Volegov, K. Widmann, D. C. Wilson and A. B. Zylstra
Phys. Plasmas **21**, 112706 (2014)

9. T. Ma, P. K. Patel, N. Izumi, P. T. Springer, M. H. Key, L. J. Atherton, L. R. Benedetti, D. K. Bradley, D. A. Callahan, P. M. Celliers, C. J. Cerjan, D. S. Clark, E. L. Dewald, S. N. Dixit, T. Do¨ ppner, D. H. Edgell, R. Epstein, S. Glenn, G. Grim,3 S. W. Haan, B. A. Hammel, D. Hicks, W. W. Hsing, O. S. Jones, S. F. Khan, J. D. Kilkenny,4 J. L. Kline,3 G. A. Kyrala,3 O. L. Landen, S. Le Pape, B. J. MacGowan, A. J. Mackinnon, A. G. MacPhee, N. B. Meezan, J. D. Moody, A. Pak, T. Parham, H.-S. Park, J. E. Ralph, S. P. Regan, B. A. Remington, H. F. Robey, J. S. Ross, B. K. Spears, V. Smalyuk, L. J. Suter, R. Tommasini, R. P. Town, S. V. Weber, J. D. Lindl, M. J. Edwards, S. H. Glenzer, and E. I. Moses, Phys. Rev. Lett. **111**, 085004 (2013)

10. T. R. Dittrich, O. A. Hurricane, D. A. Callahan, E. L. Dewald, T. Döppner, D. E. Hinkel, L. F. Berzak Hopkins, S. Le Pape, T. Ma, J. L. Milovich, J. C. Moreno, P. K. Patel, H.-S. Park, B. A. Remington, and J. D. Salmonson, Phys. Rev. Lett. **112**, 055002 (2014).

11. O. A. Hurricane, D. A. Callahan, D. T. Casey, P. M. Celliers, C. Cerjan, E. L. Dewald, T. R. Dittrich, T. Do¨ppner, D. E. Hinkel, L. F. Berzak Hopkins, J. L. Kline, S. Le Pape, T. Ma, A. G. MacPhee, J. L. Milovich, A. Pak, H.-S. Park, P. K. Patel, B. A. Remington, J. D. Salmonson, P. T. Springer and R. Tommasini, Nature **506**, 343 (2014).

12. H.-S. Park, O. A. Hurricane, D. A. Callahan, D. T. Casey, E. L. Dewald, T. R. Dittrich, T. Döppner, D. E. Hinkel, L. F. Berzak Hopkins, S. Le Pape, T. Ma, P. K. Patel, B. A. Remington, H. F. Robey, and J. D. Salmonson, Phys. Rev. Lett. **112**, 055001 (2014).

13. V. A. Smalyuk, D. T. Casey, D. S. Clark, M. J. Edwards, S. W. Haan, A. Hamza, D. E. Hoover, W. W. Hsing, O. Hurricane, J. D. Kilkenny, J. Kroll, O. L. Landen, A. Moore, A.

Nikroo, L. Peterson, K. Raman, B. A. Remington, H. F. Robey, S. V. Weber, and K. Widmann, Phys. Rev. Lett. 112, 185003 (2014).

14. D. T. Casey, V. A. Smalyuk, K. S. Raman, J. L. Peterson, L. Berzak Hopkins, D. A. Callahan, D. S. Clark, E. L. Dewald, T. R. Dittrich, S. W. Haan, D. E. Hinkel, D. Hoover, O. A. Hurricane, J. J. Kroll, O. L. Landen, A. S. Moore, A. Nikroo, H.-S. Park, B. A. Remington, H. F. Robey, J. R. Rygg, J. D. Salmonson, R. Tommasini, and K. Widmann, Phys. Rev. E **90**, 011102 (2014).

15. K. S. Raman, V. A. Smalyuk, D. T. Casey, S. W. Haan, D. E. Hoover, O. A. Hurricane, J. J. Kroll, A. Nikroo, J. L. Peterson, B. A. Remington, H. F. Robey, D. S. Clark, B. A. Hammel, O. L. Landen, M. M. Marinak, D. H. Munro, K. J. Peterson and J. Salmonson, Phys. Plasmas 21, 072710 (2014).

16. Smalyuk, private communication (2014) (DPP)

17. Weber, private communication (2014) (DPP)

18. K. L. Sequoia, H. Huang, R. B. Stephens, K. A. Moreno, K. C. Chen, and A. Nikroo, *Fusion Science and Technology **59**, 35 (2011).*

19. H. YASUDA, "Plasma Polymerization," Chapter 6, Academic Press, Orlando, FL, (1985).

20. A. Nikroo, D. G. Czechowicz, E. R.Castillo, and J. M. Pontelandolfo, Fusion Science and Technology **41**, 214 (2002).

21. T.R. GENGENBACH, Z.R. VASIC, R.C. CHATEILER, and H.J. GRIESSER, "A Multi-Technique Study of the Spontaneous Oxidation of n-Hexane Plasma Polymer," J. Polym. Sci. A 32, 1399 (1994).

22. H. Huang, D. M. Haas, Y. T Lee, J. J. Wu, K. A. Moreno, R. B. Stephens, A. Nikroo, M. Stadermann, S. D. Bhandarkar*, Fusion Science and Technology **63**, 142 (2013).*

23. M. C. Akin, Z. Jenei, M. J. Lipp, W. J. Evans, and R. Chau, "Handling and characterization of glow-discharge polymer samples for the light gas gun" (2014).

24. H. Azechi, private communication (2013).

25. G. B. Zimmerman and W. L. KRUER, *Comments Plasma Phys. Controlled Fusion* **2**, 51 (1975).

26. D. S. Clark, J. L. Milovich, D. E. Hinkel, J. D. Salmonson, J. L. Peterson, L. F. Berzak Hopkins, D. C. Eder, S. W. Haan, O. S. Jones, M. M. Marinak, H. F. Robey, V. A. Smalyuk and C. R. Weber, Phys. Plasmas 21, 112705 (2014).

27. A. MacPhee, private communication (APD DPP) (2014).

28. J. L. Peterson, D. S. Clark, L. P. Masse, and L. J. Suter, Phys. Plasmas 21, 092710 (2014).

29. A. Nikroo and J. M. Pontelandolfo, *Fusion Technology* **38**, 58 (2000).

30. S. W. Haan, J. Atherton, D. S. Clark, B. A. Hammel, D.A. Callahan, C.J. Cerjan, E.L. Dewald, S. Dixit, M.J. Edwards, S. Glenzer, S.P. Hatchett, D. Hicks, O.S. Jones, O.L. Landen, J.D. Lindl, M.M. Marinak, B.J. MacGowan, A.J. MacKinnon, N.B. Meezan, J.L. Milovich, D.H. Munro, H.F. Robey, J.D. Salmonson, B.K. Spears, L.J. Suter, R.P. Town, S.V. Weber, J.L. Kline, and D.C. Wilson, *Fusion Science and Technology **63**, 67 (2013).*

31. Y. T. Lee, A. Q. L. Nguyen, H. Huang, K. A. Moreno, K. C. Chen, C. Chen, M. A. Johnson, J. D. Hughes, R. C. Montesanti, and D. W. Phillion, *Fusion Science and Technology* **55**, 405–410 (2009).

32. C. A. Iglesias and F. J. Rogers, *Astrophys. J.* **464**, 943 (1996).

33. D. A. Young and E. M. Corey, J. Appl. Phys. **78**(6), 3748 (1995).

34. R. More, K. Warren, D. Young, and G. Zimmerman, Phys. Fluids **31**, 3059 (1988).

35. L. X. Benedict, T. Ogitsu, A. Trave, C. J. Wu, P. A. Sterne, and E. Schwegler, Phys. Rev. B 79, 064106 (2009).

36. S. Pollaine and S. Hatchett, *Nucl. Fusion* **44**, 117 (2004).

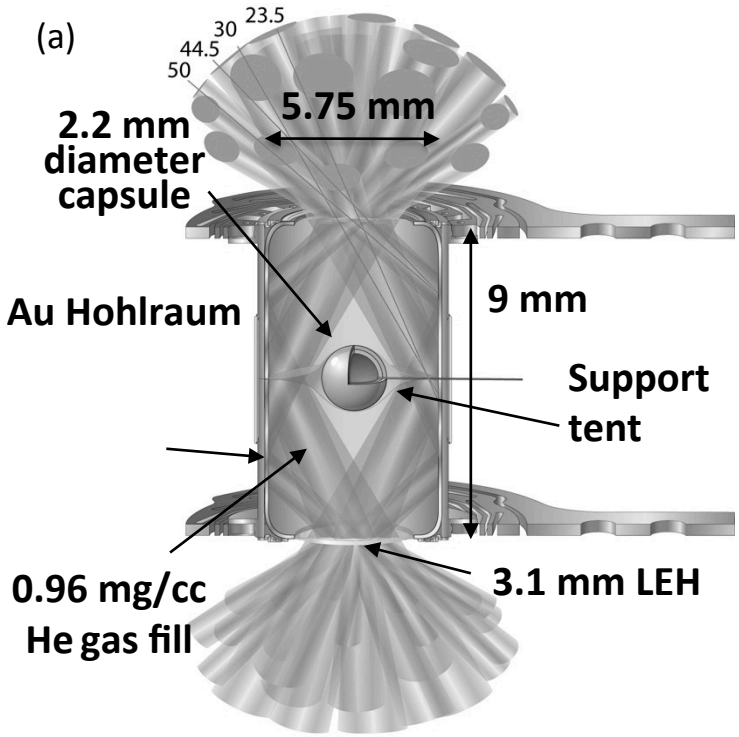

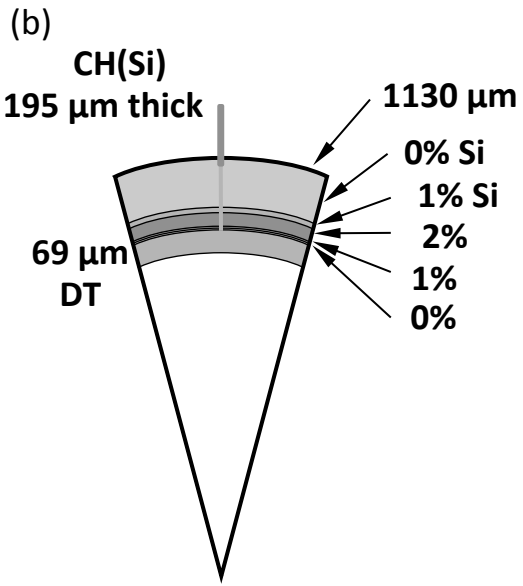

Fig. 1. Ignition target. (a) The Au hohlraum enclosing the central spherical capsule. Forty-eight "quads" of laser beams enter at indicated angles, and Si paddles support the hohlraum. (b) Pie diagram of the central capsule.

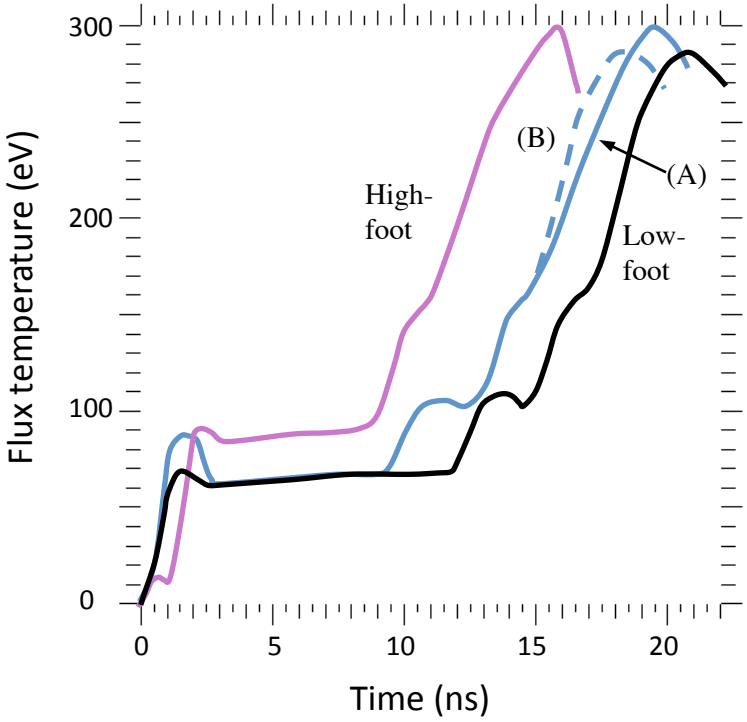

Fig. 2. Hohlraum drive temperatures used for this work. Low foot drive is based on post-shot model for shot N120329, with final rise reoptimized for ignition velocity; high-foot is model for shot N130927; "high-picket" pulse A is from Clark per ref. 26; "high-picket" pulse B has reoptimized final rise for higher velocity.

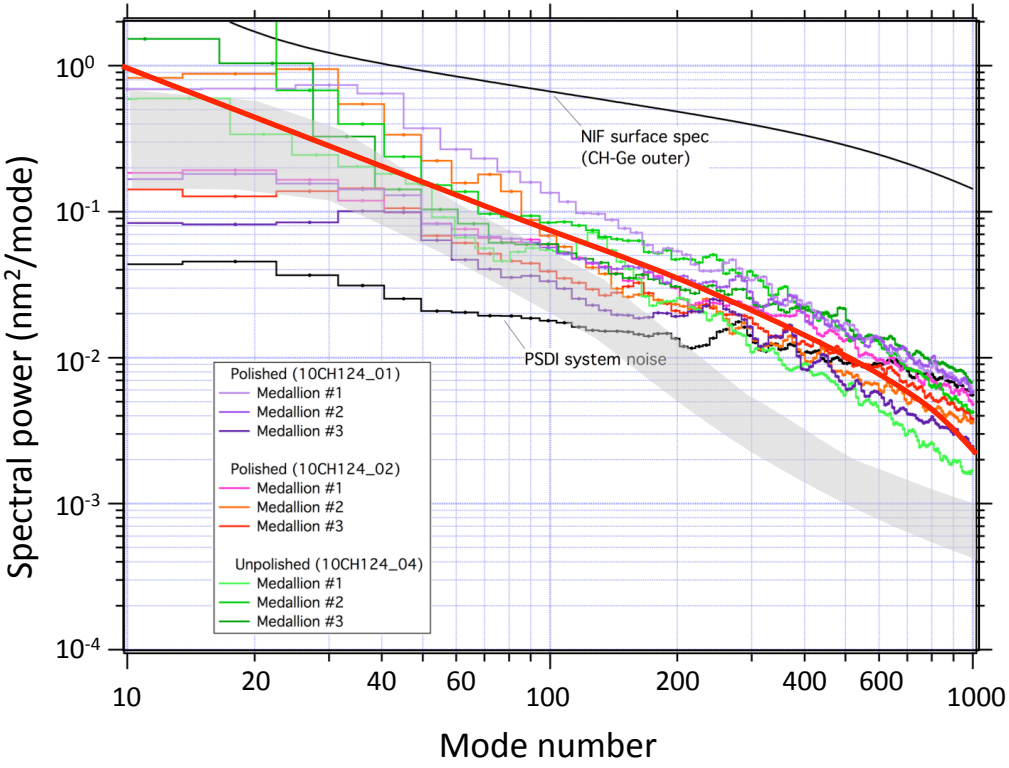

Fig. 3. Interferometric measurements of column density modulations in GDP plastic, expressed as a power spectrum (nm^2) of ρR-equivalent surface roughness. Data is shown for three locations each, on three shells. Curve labeled "NIF surface spec" is the maximum allowed surface roughness. The noise curve for the equivalent surface roughness measurements is also shown. The gray semi-transparent band is the average of the curves from Fig. 4, copied here for comparison, and the red line is a nominal test case given by eq. (3).

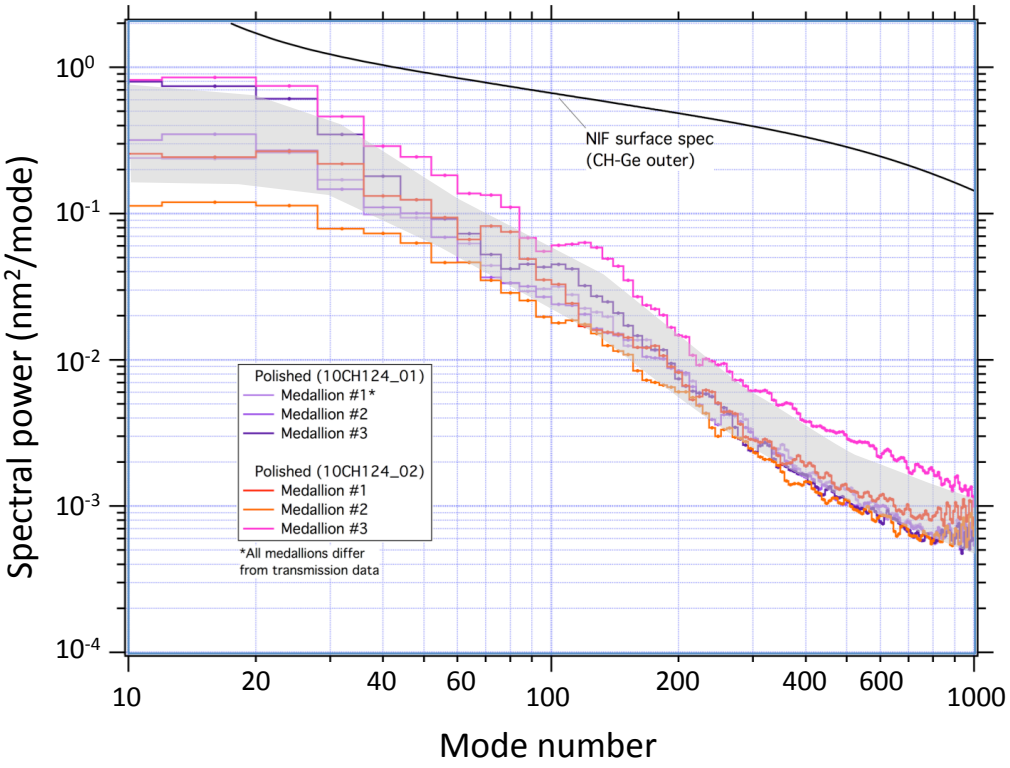

Fig. 4. Actual outer surface roughness power spectrum for two of the shells shown in Fig. 3. Gray band is average ± rms, smoothed, to facilitate comparison with Fig. 3.

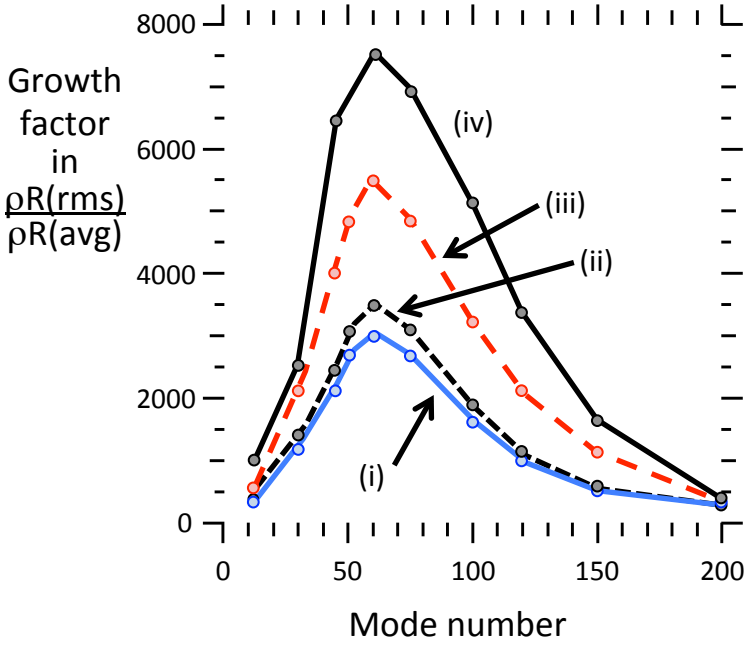

Fig 5. Growth in column density of modulations seeded by: (i) conventional outer surface ripples; (ii) density modulations only, with spatial dependence per eq. (4); (iii) oxygen modulations only, with no density modulation, where the initial oxygen modulation matches that of curve (iv); and (iv) oxygen modulations with spatial dependence per eq. (4) and density following the oxygen per eq. (2).

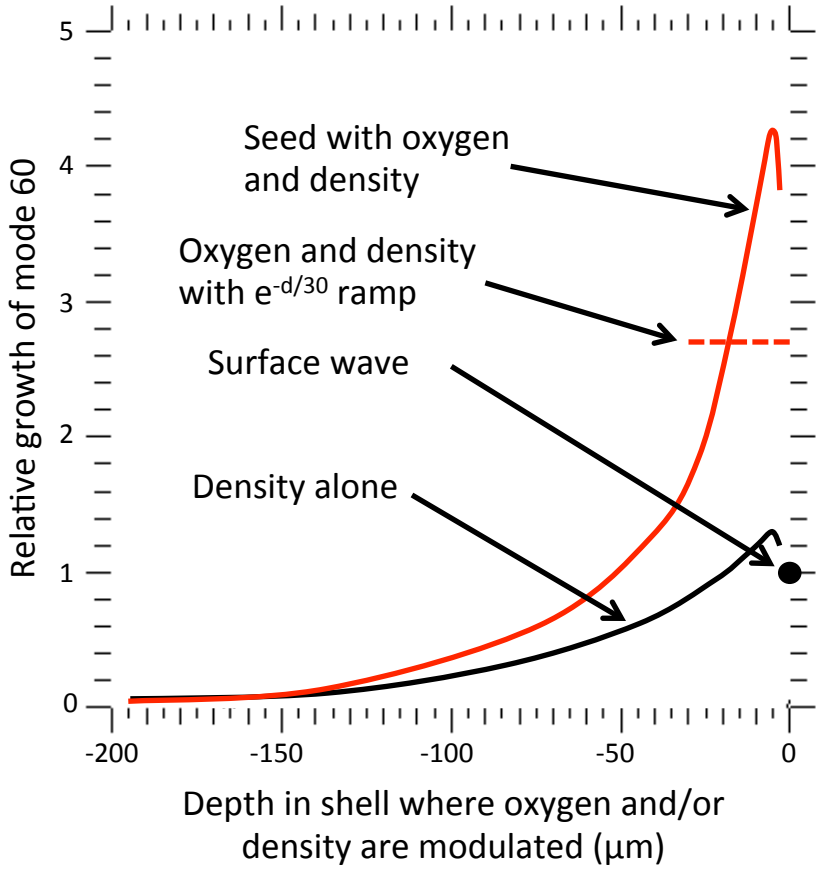

Fig 6. Relative growth of mode 60 when seeded by density or oxygen modulations radially placed in a micron-scale step, initially at the depth corresponding to the x-axis. The dot on the right is the growth of a surface ripple, normalized to the same initial ρR modulation. The curves are seeded, as indicated, with density modulations alone, or with oxygen and the accompanying density. Growth seeded by the exponential ramp, eq. (4), is also indicated on the right.

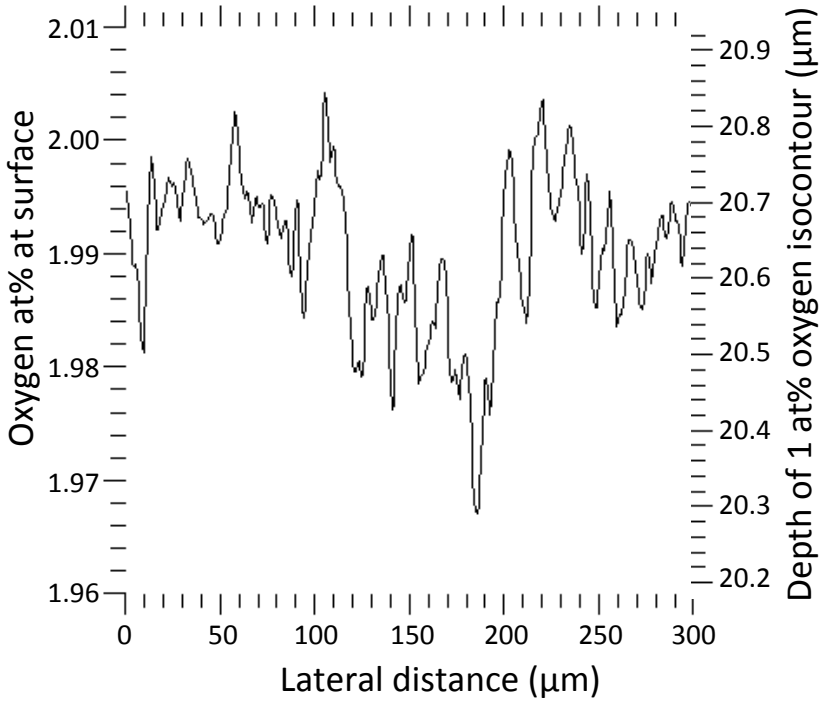

Fig 7. Typical real-space features of the oxygen profile considered in Sec IV. The power spectrum of the integrated column density is the nominal test case eq. (3), indicated in Fig. 2. Oxygen radial profile is per eq. (4), extended to multiple modes. The same curve represents both the oxygen atomic percent at the surface, left scale, and the depth of the 1 at% oxygen contour, right scale. Of course in reality the oxygen at 20μm burial would not be perfectly correlated with surface level. The surface content is slightly below the average of 2% because of low-mode modulations that are not captured by this short line segment.

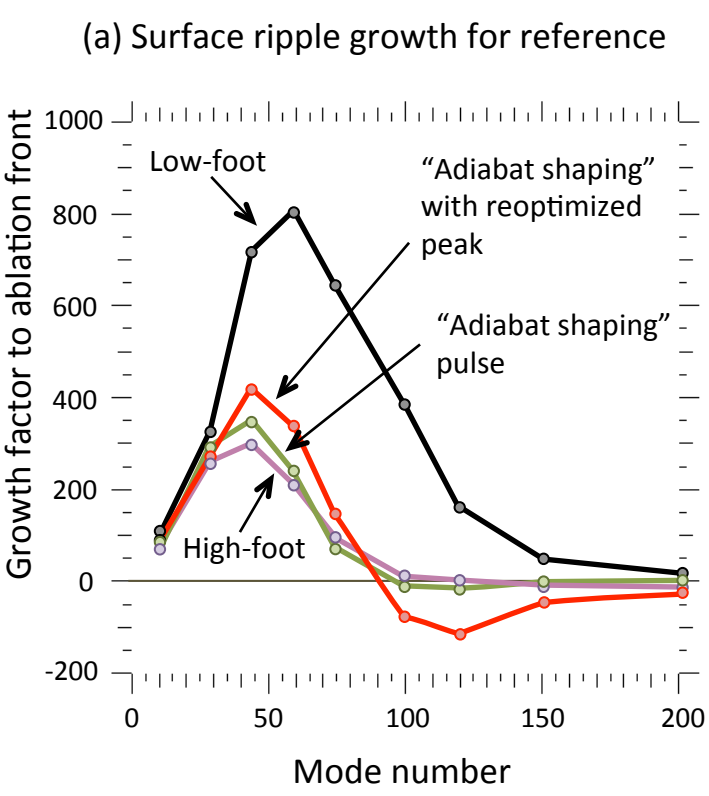

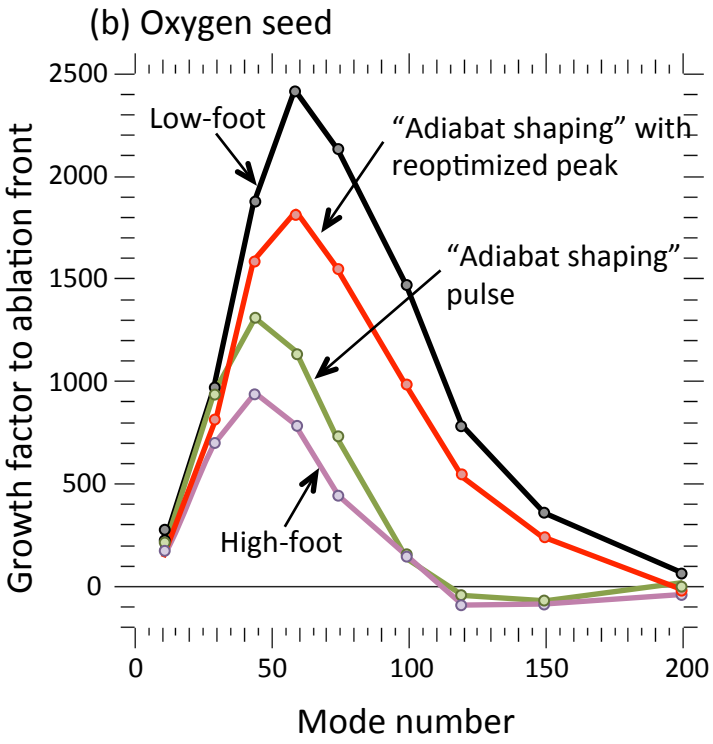

Fig 8. (a) Growth of conventionally seeded surface ripples, for the four drives shown in Fig. 2, as calculated with the code and setup used for this work. (b) Growth of oxygen modulations for these same four cases, using the same setup as for Fig. 5. In this case the final amplitudes are ablation front amplitudes as conventionally shown for surface growth as in (a), with the growth factor denominator normalized to a surface ripple with the same column density.

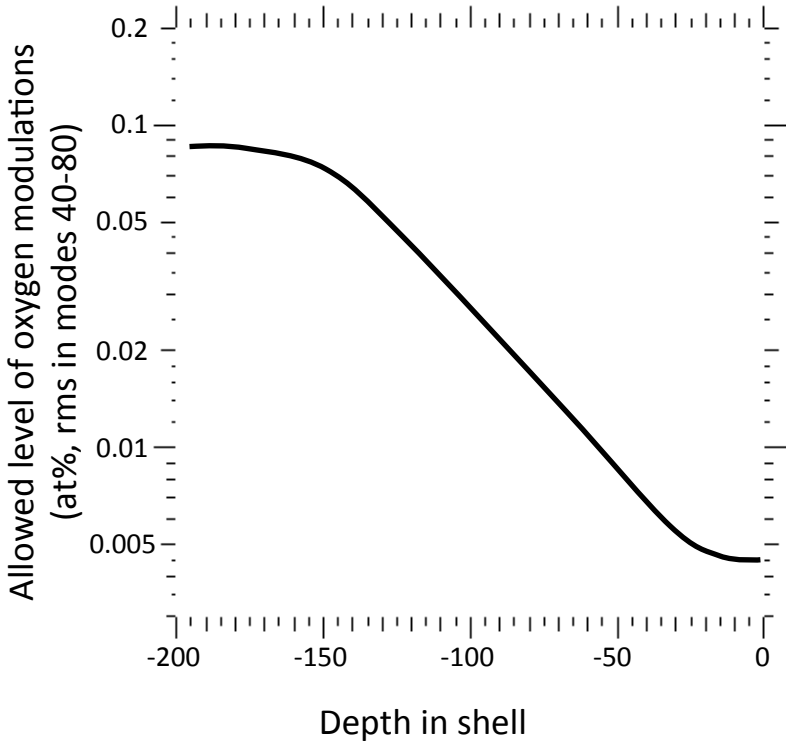

Fig 9. Draft requirement on allowed level of oxygen modulations. In the transverse direction, this is the rms in modes 40-80. In the radial direction, this assumes persistence of the phase of the transverse modulations over a 20 μm correlation length. Modulations with shorter radial correlation length can be larger, in proportion to (correlation length)$^{-1}$.